PERGAMON

International Journal of Heat and Mass Transfer 42 (1999) 803–819

International Journal of HEAT and MASS TRANSFER

Analysis of transient heat/mass transfer and adsorption/desorption interactions

A. G. Fedorov, R. Viskanta*

Heat Transfer Laboratory, School of Mechanical Engineering, Purdue University, West Lafayette, IN 47907, U.S.A.

Received 3 November 1997; in final form 15 July 1998

Abstract

A transient, two-dimensional theoretical analysis of combined heat and mass transfer and adsorption/desorption dynamics is presented to investigate the effects of the local non-linear interactions between heat and mass transfer and adsorption/desorption as the surface phenomena. A honeycomb adsorption column is used as a model system. The simplified statistical mechanics (SLD) model is employed to simulate an adsorption equilibrium on the flat walls of the honeycomb adsorbent. Appropriate surface boundary conditions for heat and mass transfer in the presence of adsorption/desorption are formulated. Model predictions are compared with available experimental data for adsorption of water vapor in a honeycomb column, and very good agreement is obtained between the numerical simulations of the system dynamics and the measurements. The findings demonstrate that it is important to correctly account for heat and mass transfer and adsorption/desorption interactions in the system.

Nomenclature

A specific surface area
C concentration
c_p specific heat at constant pressure
D mass diffusivity
D_h hydraulic diameter of the unit cell
d spacing between walls of the unit cell
ΔH differential enthalpy of adsorption
H width of the channel (see Fig. 1)
k thermal conductivity
L length of the channel (see Fig. 1)
p pressure
q heat flux
Re_{D_h} Reynolds number based on hydraulic diameter, $\rho u_i D_h/\mu$
T temperature
t time or wall thickness of the unit cell
u, v velocity components in x- and r-directions, respectively
w thickness of the channel wall (see Fig. 1)
x, r spatial coordinates (see Fig. 1).

Greek symbols

Γ amount adsorbed or generalized diffusivity in equation (17)
μ dynamic viscosity
ρ density
ω mass fraction of adsorbable species.

Subscripts

b bulk quantity
g quantity at the gas phase
h sensible heat transfer
i inlet
m latent (due to adsorption/desorption) heat transfer
w quantity at solid (adsorbent wall) phase
0 initial conditions
□ square-shaped unit cell
○ circular tube
‖ parallel plate channel.

Superscript

• refers to partial derivative in time.

* Corresponding author. Fax: +1 765 494 0539

0017–9310/98/$—see front matter
PII: S0017–9310(98)00228–2

1. Introduction

Numerous technological processes ranging from gas separation and drying to impurity removal in pollution control and recovery of radiactive wastes have been developed based on physical adsorption [1,2]. Adsorption/desorption is a physical process which leads to enrichment/depletion of one or more gaseous components in the interfacial layer [3]. Significant heat and mass flux fluxes arise at the gas/solid interface when adsorption/desorption takes place.

Transient heat and mass transfer during adsorption/desorption have received considerable attention and an excellent review is available [4]. Up to date literature citations can be found in the more recent publication [5]. In summary, the majority of studies have analyzed one-dimensional heat and mass transfer and adsorption in the packed beds. The local heat and mass transfer coefficients were extracted from the steady-state empirical correlations, and the analogy between heat and mass transfer processes were commonly assumed. No theoretical or experimental studies dealing with the local nonlinear heat/mass transfer and adsorption/desorption interactions and their effect on the system dynamics have been performed or, at least, reported in the literature. Few authors [6–9] have employed the two-dimensional heat and mass transfer models to simulate adsorption dynamics of the packed bed, but they focused their attention on the effect of transverse mass diffusion, heat conduction, and heat losses through the walls.

Clearly, validity of heat and mass transfer analogy is questionable in the presence of adsorption/desorption at the adsorbent walls and, in general, the local non-linear interactions between heat/mass transfer and adsorption/desorption cannot be neglected. For example, during adsorption/desorption phase of the system dynamics, the net mass inflow/outflow of adsorbable species exists at the wall. This phenomenon disturbs the temperature and adsorbate concentration fields in the immediate vicinity of the adsorbent solid and, thus, influences greatly the equilibrium conditions for adsorption/desorption. In turn, a change in the local equilibrium conditions leads to changes in adsorption/desorption dynamics and associated thermal effects.

This paper presents an analysis of the heat/mass transfer and adsorption/desorption dynamics. The aim is to gain understanding of local nonlinear interactions between heat/mass transfer and adsorption/desorption processes and their effects on the overall system dynamics. To this end, the transient two-dimensional model for combined heat/mass transfer and adsorption/desorption dynamics employing a conjugate formulation is developed. Dynamics of the honeycomb adsorption column is simulated, and numerical results are reported for the water vapor as an adsorbable species. Availability of the detailed experimental data of transient temperatures, adsorbate concentrations, and local heat fluxes during adsorption/desorption of water vapor in the honeycomb adsorbent [17] provides an excellent opportunity to validate the theoretical model developed.

2. Analysis

2.1. Physical model, assumptions and model equations

Consider a cylindrical or parallel-plate rectangular channel shown schematically in Fig. 1. This channel represents a two-dimensional analog of the square-shaped unit cell of the honeycomb adsorption column [5]. As the adsorbate/carrier gas mixture enters the channel, a fraction of the adsorbable species is adsorbed by the chemically active adsorbent solid. The adsorbed species forms a very thin (of the order of several nanometers) stagnant film in the vicinity of the solid wall due to presence of short-ranged attractive forces between solid and adsorbate molecules. The equilibration time for adsorption/desorption processes is very short (of the order of several μs) [10] compared to the time frame for the process of interest (of the order of several min). Therefore, the advective and diffusive mass transfer of the adsorbable species from the bulk mixture to the adsorbate film is considered to be the rate controlling process. Adsorption/desorption processes are accompanied by the significant heat source/sink [1], and this leads to the strong coupling between heat and mass transfer. Also, the amount of the adsorbable species adsorbed in the film depends on the temperature at the solid wall/flowing mixture interface. Hence, heat transfer by conduction in the solid adsorbent walls could influence greatly the local equilibrium conditions and needs to be accounted for adequate description of the process.

A theoretical model for combined heat and mass transfer in conjunction with adsorption/desorption in the cylindrical/parallel-plate channel is developed under the following main assumptions: (1) the transport processes are considered to be transient and two-dimensional; (2) the flow is incompressible and laminar since the hydraulic diameter of the honeycomb unit cell is of the order of several millimeters and a typical flow Reynolds number is of the order of one hundred; (3) the body forces (e.g., buoyancy force) are neglected in comparison to pressure force (forced convection regime); (4) thermal diffusion (Soret), diffusion-thermo (Dufour) and interdiffusion effects are neglected in comparison to advection; (5) viscous heat dissipation, pressure work, and thermal radiation are neglected in comparison to advection (the typical operation temperature is below 100°C); (6) the amount of adsorbable species adsorbed/desorbed per unit time is negligibly small in comparison to mass flow rate of the carrier gas and the adsorbed film is considered to be infinitesimally thin; and (7) the solid adsorbent is

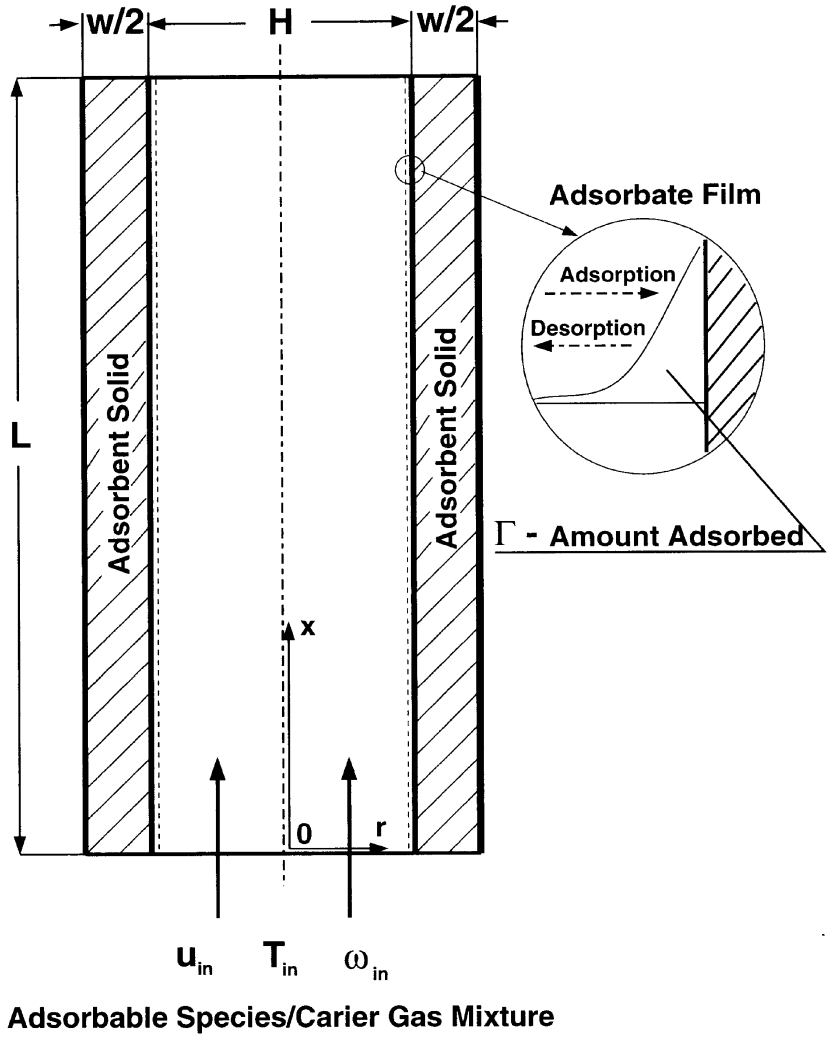

Fig. 1. Schematic of the physical arrangement and the coordinate system.

considered to be non-porous, i.e., neither macropores nor micropores are present.

Under the assumptions given above, the conservation equations of mass, momentum, energy, and species for the model can be written as follows (see Fig. 1 for coordinate system):

Conservation of mass (continuity):

$$\frac{\partial \rho}{\partial t}+\frac{\partial(\rho u)}{\partial x}+\frac{1}{r^i}\frac{\partial(r^i \rho v)}{\partial r}=0 \tag{1}$$

Conservation of x-momentum:

$$\frac{\partial(\rho u)}{\partial t}+\frac{\partial(\rho u u)}{\partial x}+\frac{1}{r^i}\frac{\partial(r^i \rho v u)}{\partial r} = -\frac{\partial p}{\partial x}+\frac{\partial}{\partial x}\left(\mu\frac{\partial u}{\partial x}\right)+\frac{1}{r^i}\frac{\partial}{\partial r}\left(r^i \mu\frac{\partial u}{\partial r}\right) \tag{2}$$

Conservation of r-momentum:

$$\frac{\partial(\rho v)}{\partial t}+\frac{\partial(\rho u v)}{\partial x}+\frac{1}{r^i}\frac{\partial(r^i \rho v v)}{\partial r} = -\frac{\partial p}{\partial r}+\frac{\partial}{\partial x}\left(\mu\frac{\partial v}{\partial x}\right)+\frac{1}{r^i}\frac{\partial}{\partial r}\left(r^i \mu\frac{\partial v}{\partial r}\right)-i\mu\frac{v}{r^2} \tag{3}$$

Conservation of adsorbable species:

$$\frac{\partial(\rho \omega)}{\partial t}+\frac{\partial(\rho u \omega)}{\partial x}+\frac{1}{r^i}\frac{\partial(r^i \rho v \omega)}{\partial r}$$

$$= \frac{\partial}{\partial x}\left(\rho D\frac{\partial \omega}{\partial x}\right) + \frac{1}{r^i}\frac{\partial}{\partial r}\left(r^i \rho D\frac{\partial \omega}{\partial r}\right) \quad (4)$$

Conservation of energy for gas:

$$\frac{\partial(\rho c_{pg} T_g)}{\partial t} + \frac{\partial(\rho u c_{pg} T_g)}{\partial x} + \frac{1}{r^i}\frac{\partial(r^i \rho v c_{pg} T_g)}{\partial r} = \frac{\partial}{\partial x}\left(k_g \frac{\partial T_g}{\partial x}\right) + \frac{1}{r^i}\frac{\partial}{\partial r}\left(r^i k_g \frac{\partial T_g}{\partial r}\right) \quad (5)$$

Conservation of energy for solid (adsorbent):

$$\frac{\partial(\rho_w c_w T_w)}{\partial t} = \frac{\partial}{\partial x}\left(k_w \frac{\partial T_w}{\partial x}\right) + \frac{1}{r^i}\frac{\partial}{\partial r}\left(r^i k_w \frac{\partial T_w}{\partial r}\right) \quad (6)$$

Note that the above formulation is valid for both cylindrical ($i = 1$) and Cartesian ($i = 0$) coordinate systems, and the variation of thermophysical properties of the adsorbable species/carrier gas mixture with both local temperature and composition is accounted for. Also, in contrast to the one-dimensional models [4], there are no mass and heat sources in the mass and energy conservation equations, (4)–(6). This is because adsorption/desorption is a surface phenomena and, therefore, the solutal and thermal effects associated with adsorption/desorption should be incorporated into the boundary conditions.

2.2. Initial and boundary conditions

Initially, the channel is considered to be filled with a quiescent mixture which is in equilibrium with the channel walls at the temperature T_0 and consists of the adsorbable species of the mass fraction ω_0, i.e.,

$$u = 0, v = 0, T_g = T_w = T_0, \omega = \omega_0 \quad \text{at } t = 0 \quad (7)$$

Then, the preheated ($T_i > T_0$) and adsorbable species rich ($\omega_i > \omega_0$) mixture is introduced at the inlet to the channel at the constant rate, i.e.,

$$u = u_i, T_g = T_i, \omega = \omega_i \quad \text{at } x = 0 \quad (8)$$

It is assumed that the gradients of the mixture axial velocity, mixture and wall temperatures, and species mass fraction vanish at the exit of the channel, i.e.,

$$\frac{\partial u}{\partial x} = \frac{\partial T_g}{\partial x} = \frac{\partial T_w}{\partial x} = \frac{\partial \omega}{\partial x} = 0 \quad \text{at } x = L \quad (9)$$

The symmetry boundary conditions are imposed for all transport variables at the centerline of the channel, i.e.,

$$v = \frac{\partial u}{\partial r} = \frac{\partial T_g}{\partial r} = \frac{\partial \omega}{\partial r} = 0 \quad \text{at } r = 0 \quad (10)$$

The surface of solid walls at the inlet to the channel ($x = 0$) is assumed to be in the thermal equilibrium with the entering mixture and the adiabatic condition is adopted for the outer channel surface [$r = (H+w)/2$], i.e.,

$$T_w = T_i \quad \text{at } x = 0 \quad (11)$$

and

$$\frac{\partial T_w}{\partial r} = 0 \quad \text{at } r = (H+w)/2 \quad (12)$$

respectively.

The no-slip boundary condition is used for the axial velocity component (u),

$$u = 0 \quad \text{at } r = H/2 \quad (13)$$

The transverse velocity component (v) of the mixture as well as the boundary conditions for species conservation equation at the channel wall ($r = H/2$) are obtained by assuming the adsorbate film to be infinitesimally thin and semipermeable [11]; that is, the solubility of the carrier gas in the adsorbate film is negligibly small, and the mass flux of the air is zero in the overall mass balance at the film interface,

$$\dot{\Gamma} = -\frac{\rho D}{1-\omega}\frac{\partial \omega}{\partial r} \quad \text{or } v = \dot{\Gamma}/\rho = -\frac{D}{1-\omega}\frac{\partial \omega}{\partial r} \quad \text{at } r = H/2 \quad (14)$$

Here, Γ represents a surface excess of adsorbate or, in other words, an equilibrium amount of adsorbable species adsorbed in kg per unit surface area of the solid wall. Hence, $\dot{\Gamma}$ denotes the net mass flux at the wall induced by changes in the amount adsorbed in the film with time. Equation (14) states that if adsorption occurs and an equilibrium amount adsorbed increases ($\dot{\Gamma} > 0$) then the mass fraction of adsorbable species decreases in the direction towards the wall ($\partial\omega/\partial r < 0$), and the adsorption induced transverse velocity is positive ($v > 0$), i.e., directed towards the wall. Clearly, the opposite is true in the case of desorption ($\dot{\Gamma} < 0$). Note that the equilibrium amount adsorbed (Γ) depends on the local mixture temperature and species mass fraction at the film interface (i.e., at the wall) as well as on the characteristics of the adsorbate–adsorbent force interactions. This quantity is determined from the simplified local density (SLD) model [12, 13].

The adsorption/desorption processes are accompanied by the release/consumption of the significant amount of heat. Therefore, by assuming the adsorbed film to be infinitesimally thin, the conjugate boundary conditions at the adsorbent solid wall/flowing mixture interface are given by

$$T_g = T_w \quad \text{at } r = H/2 \quad (15)$$

$$-k_g \frac{\partial T_g}{\partial r} + \dot{\Gamma}(-\Delta H) = -k_w \frac{\partial T_w}{\partial r} \quad \text{at } r = H/2 \quad (16)$$

It should be noted that adsorption from the gaseous phase is invariably exothermic [1] and, therefore, the enthalpy of adsorption ΔH is a negative quantity ($-\Delta H > 0$).

A nonlinearity is introduced into the analysis by the presence of adsorption/desorption [see equations (14)

and (16)]. A scaling analysis performed [14] indicates that no uniquely defined scales for the temperature and adsorbate concentrations should exist or, in other words, different scales may be appropriate during different stages of the adsorption/desorption process. Therefore, no attempt has been made to non-dimensionalize the model equations.

2.3. Method of solution

The model conservation equations (all, but continuity) are of the parabolic type and can be expressed in the general form,

$$\frac{\partial}{\partial t}(\rho\phi)+\frac{1}{x_i^j}\frac{\partial}{\partial x_i}(x_i^j\rho u_i\phi)=\frac{1}{x_i^j}\frac{\partial}{\partial x_i}\left(x_i^j\Gamma\frac{\partial\phi}{\partial x_i}\right)+S \qquad (17)$$

where ϕ represents any dependent variable, i.e., velocity components, mass fraction, temperature, etc. A fully implicit, absolutely stable Euler method with the constant time steps is employed to integrate eqn (17) in time. The governing partial differential equations along with the boundary conditions are discretized over the spatial coordinates by means of the control volume integration technique [15]. The resulting finite-difference approximation of derivatives produces a system of linear algebraic equations which are, then, solved by using a line-by-line iterative method. The method solves a line of nodes by applying the three-diagonal matrix inversion algorithm and sweeps the domain of the integration in different directions along the coordinate exes. The SIMPLER algorithm is employed to solve the coupled system of conservation equations in primitive or dimensional variables, and this is discussed in detail by Patankar [15]. Suffice it to mention that the dependent variables u, v, ω. T_g, and T_w are first underrelaxed by a factor of 0.7 and, then, the relaxation factor is gradually increased up to 1.0 in order to obtain the converged solution at the each time step.

The highly compressed nonuniform grid near the channel walls was adopted in order to properly resolve viscous shear layers. Sine-in-power distribution was shown to be very reliable even for the turbulent shear flows at relatively high Reynolds numbers [16] and, therefore, is used in this study. The grid nodes were also concentrated along the axial direction in the entrance of the channel for the sake of the proper resolution of the flow, thermal and solutal development regions.

The computer program was extensively evaluated by comparing with available theoretical predictions and experimental data for some limiting cases [14]. Grid independence of results in spatial variables was established by employing different size meshes, ranging in size from 100×15 to 300×35 in x- and r-directions, respectively. A sensitivity of the numerical calculations to the changes in the time step has also been assessed by performing simulations with time increments of 10, 5, and 1 s. The computer time required for transient calculations increases considerably as the number of grid nodes increases. This stimulated a search for the numerical grid with a smallest possible number of nodes but still satisfying the acceptable accuracy requirements. The results of the grid sensitivity study showed that the simulations based on the grid with 200 nodes in the x-direction and 25 nodes in the r-direction and time step of 5 s provided satisfactory numerical accuracy [14]. Thus, all transient computations of heat and mass transfer and adsorption dynamics were performed on the grid 200×25 with a time step of 5 s.

3. Results and discussion

3.1. Comparison between predictions and experimental data

The dynamics of heat/mass transfer in the presence of adsorption/desorption is simulated in the case of the honeycomb adsorption column employed in the experimental studies of the Yamada and co-workers [17]. A detailed description of the experimental system and procedure can be found elsewhere [14], and only parameters and data which are directly relevant to the present theoretical analysis are provided. The experimental honeycomb column was made of complex metaloxide (TiO_2–WO_3–V_2O_5), and its thermophysical properties are summarized in Table 1. The nitrogen adsorption experiments have been performed, and the results indicate that the specific surface area occupied by the micropores is negligibly small (less than 5%) compared to the total specific surface area [14]. This means that, for all practical purposes, adsorption of the gaseous adsorbable species in the micropores can be neglected in comparison to adsorption which takes place on the flat surfaces of the honeycomb walls.

The honeycomb unit cell was $L=0.3$ m in length and square-shaped with a spacing between walls $d=2.69$ mm and a wall thickness $t=0.58$ mm. It was replaced by the cylindrical tube with an equivalent hydraulic diameter $D_h=d=H$ and wall thickness $t=$ w [14]. As a concrete example, the simulations are performed for the flow conditions characterized by the Reynolds number equal to

Table 1
Thermophysical properties of TiO_2–WO_3–V_2O_5 [17]

Physical properties	100°C	300°C	500°C
Density, ρ_w [kg/m^3]	1650	1650	1650
Specific heat, c_w [J/kg K]	821	900	950
Thermal conductivity, k_w [W/m K]	0.371	0.393	0.392

75. The initial and inlet mixture temperatures and concentrations of the adsorbable species are given in Table 2. The equilibrium amount of adsorbable species (water vapor) adsorbed at different local temperature and adsorbate mass fraction is evaluated using the simplified local density (SLD) adsorption model described elsewhere [13].

The transient distributions of the bulk mixture temperature and water vapor concentration at the different spatial locations along the cylindrical channel are shown in Figs 2 and 3, respectively. The results of numerical calculations are compared with experimental data [17]. Excellent agreement between theoretical predictions and experimental data has been obtained. Furthermore, use of the two-dimensional heat/mass transfer analysis allowed considerable improvement which produced good quantitative agreement between theoretical predictions and experimental data compared to the results obtained when a one-dimensional heat and mass transfer model was employed [5, 13]. Particularly large improvement is achieved in predicting the transient adsorbate concentration uptake. The one-dimensional model has greatly overpredicted the concentration overshoot and the time interval of an overshoot duration. This success is attributed to accounting for the local interactions between heat/mass transfer and adsorption/desorption in the framework of a two-dimensional analysis.

Table 2
Initial and inlet parameters of the mixture

T_0 [°C]	T_i [°C]	C_0 [kg/m^3]	C_i [kg/m^3]
22.5	42.5	0.0147	0.0184

The transient sensible heat fluxes at the wall $[q_h = -k_g(\partial T_g/\partial r)_w]$ at four different spatial locations along the tube are illustrated in Fig. 4. The calculated sensible heat fluxes compare well with the experimental data obtained by Yamada [17]. The maximum discrepancy between the theoretical results and measurements lies in predicting the amplitude of the second peak in the sensible heat flux at the location $x/L = 1/3$ during the desorption swing (2 min $< t <$ 14 min) and it is less than 9%. At the same time, the sensible heat fluxes during an adsorption swing (e.g., 0 min $< t <$ 2 min for $x/L = 1/3$) predicted by the 2-D heat and mass transfer

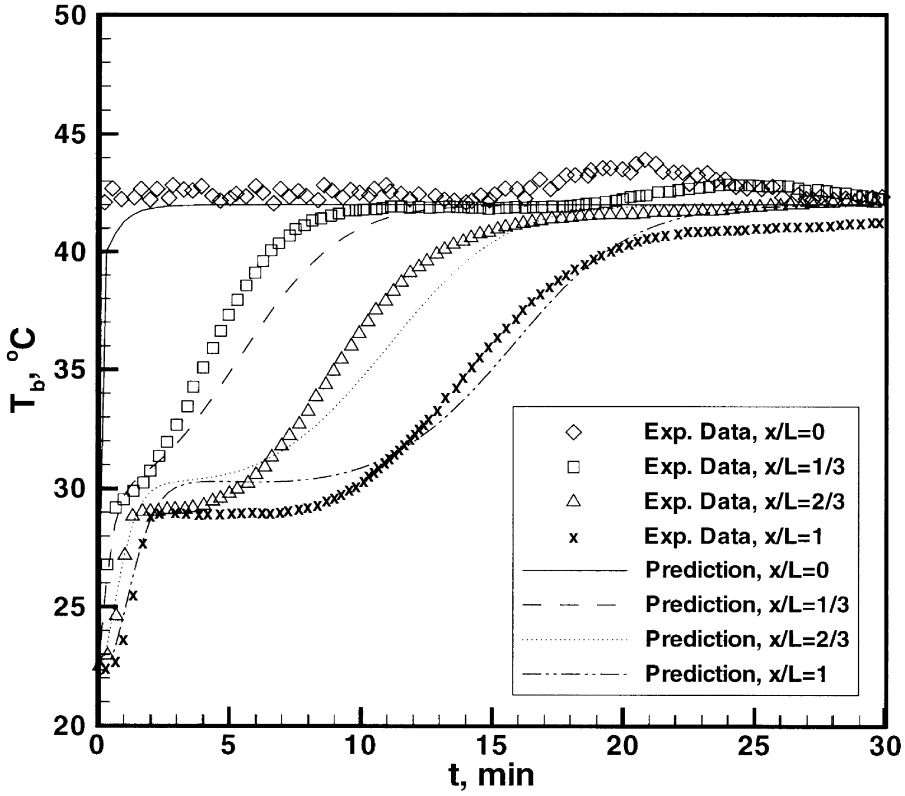

Fig. 2. Comparison of the theoretically predicted transient temperature distributions with experimental data of Yamada [17] for $Re_{D_h} = 75$.

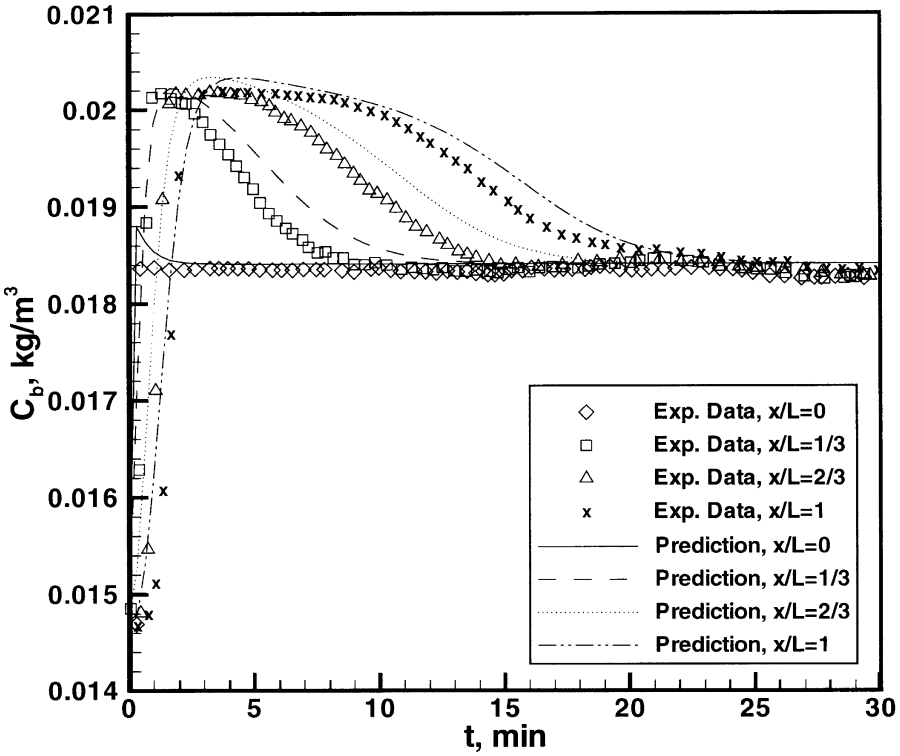

Fig. 3. Comparison of the theoretically predicted transient distributions of the adsorbable species concentration with experimental data of Yamada [17] for $Re_{D_h} = 75$.

model are in excellent agreement with the experimental data at all four locations along the tube.

To complete a discussion, the transient latent heat fluxes due to adsorption/desorption $[q_m = \rho v_w(-\Delta H) = \dot{\Gamma}(-\Delta H)]$ at different distances from the inlet are shown in Fig. 5. As expected [see eqn (16)], the latent heat fluxes are positive during an adsorption swing of the process (0 min $< t <$ 2 min for $x/L = 1/3$, for example), and negative during a desorption swing (2 min $< t <$ 14 min). Also, note that the magnitude of calculated latent heat fluxes is about 35% larger than that of the sensible heat fluxes (see Fig. 4).

3.2. Analysis of local heat and mass transfer

The instantaneous longitudinal and transverse velocity components exhibit behavior typical of the laminar tube flow ($Re_{D_h} = 75$). The profiles of the longitudinal velocity component are symmetric with respect to the centerline of the channel ($r = 0$). The maximum of the longitudinal velocity component occurs at the channel centerline, and it slightly decreases along the channel. This is because the gas temperature is higher (density is lower) at the positions close to the inlet to the channel where the temperature uptake is initially introduced (Fig. 2).

As expected, the maximum magnitude of the transverse velocity component is several orders of magnitude smaller than the longitudinal one, and it vanishes at the axis of symmetry ($r = 0$). However, unlike the longitudinal velocity, the transverse velocity does not vanish at the wall but is finite owing to the existence of the adsorption/desorption induced net mass flux at the wall [see the boundary condition, eqn (14)]. It is negative at locations where desorption occurs, and there is net mass flux away from the wall. The velocity is positive at the locations where adsorption occurs, and the net mass flux is directed towards the wall. This fact is illustrated in Fig. 6 which shows the instantaneous spatial distributions of the adsorption/desorption induced velocity at the wall at several different time instants. In fact, at a time instant $t = 2$ min for example, when the dimensionless distance x/L exceeds 0.58 (i.e., $x > 0.175$ m for $L = 0.3$ m), the transverse velocity at the wall changes its sign from negative (desorption mode) to positive (adsorption mode). Also note that in the immediate vicinity of the channel wall, the suction (adsorption induced) and blowing (desorption induced) transverse velocities are significant (Fig. 6) and, therefore, the longitudinal and transverse transports are comparable in magnitude to each other. This observation is especially important since adsorption

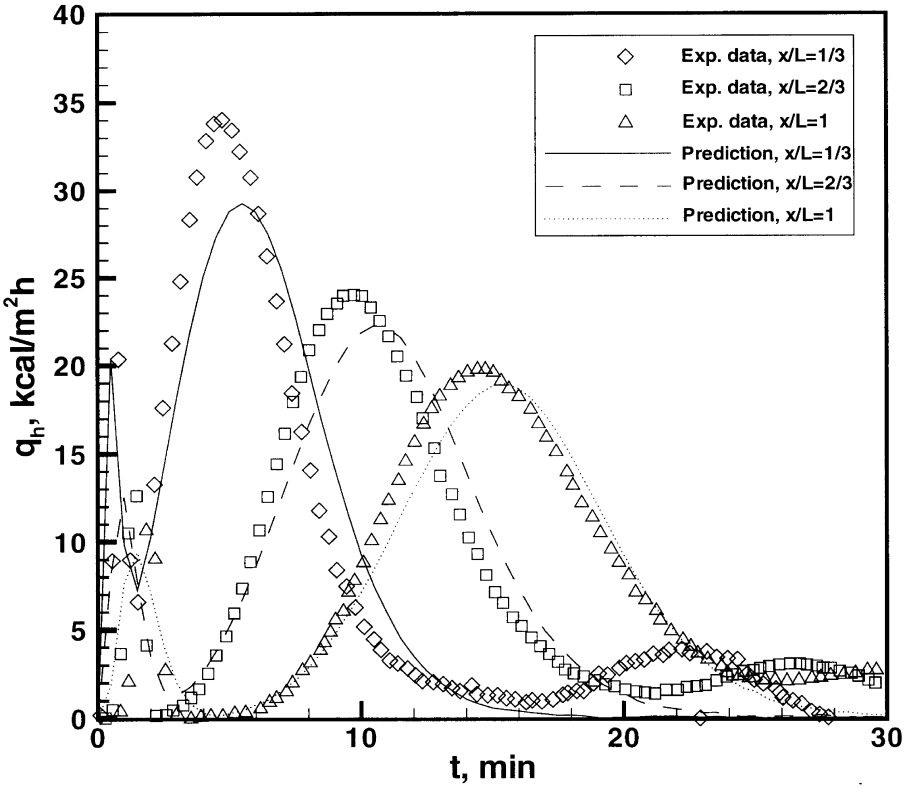

Fig. 4. Comparison of the theoretically predicted transient sensible heat fluxes with experimental data of Yamada [17] for $Re_{D_h} = 75$.

is a surface phenomenon, and an equilibrium amount of species adsorbed is strongly dependent on the local hydrodynamic, thermal, and solutal conditions close to the wall.

The temperature and adsorbable species mass fraction profiles at several locations along the channel are shown in Figs 7 and 8, respectively. For the sake of consistency, the results presented correspond to the time instant of 2 min after initiation of the process. Also, note that no attempt is made to present the results in the dimensionless form, because the conjugate character of the problem and presence of adsorption/desorption at the channel walls make the wall temperature and adsorbate mass fraction vary with time and locally along the tube. As already mentioned, this implies an absence of universal scales for the temperature and adsorbate mass fraction, which would be applicable at every stage of the process.

The magnitude of the temperature and adsorbate mass fraction decreases with an increase in the distance, because the initial temperature and mass fraction uptakes introduced at the inlet reach the locations closest to the inlet sooner than those which are further downstream. The tube wall ($r > 1.345$ mm) is virtually isothermal, owing to the relatively large thermal conductivity of the column material. As already noted in the preceding analysis of the transverse velocity profiles, desorption and adsorption occur at $x \leqslant 0.175$ m and $x > 0.175$ m, respectively. The same conclusion can be drawn from the study of the adsorbable species mass fraction profiles; the water vapor mass fraction ω is larger in the vicinity of the wall than in the bulk gas (i.e., desorption takes place and adsorbable species is released) for $x \leqslant 0.175$ m, and the opposite is true for $x > 0.175$ m (i.e., adsorption takes place and adsorbable species is consumed). Also, note that the simultaneous heating of the gas in the core by advection and cooling of the gas in the vicinity to the wall due to desorption leads to the relatively large radial temperature gradients at the location $x = 0.03$ m compared to those at locations $x \geqslant 0.18$ m where advective heating and heat release due to adsorption accompany each other.

Figure 9 shows the spatial variations of the sensible and latent (due to adsorption/desorption) heat fluxes at the wall at three different times. Recall that following the conjugate boundary condition, eqn (16), the sensible and latent heat fluxes at $r = H/2$ are defined as

$$q_h = -k_g \frac{\partial T_g}{\partial r} \quad \text{and} \quad q_m = \dot{\Gamma} \times (-\Delta H) \tag{18}$$

respectively. As already found, the maximum magnitude

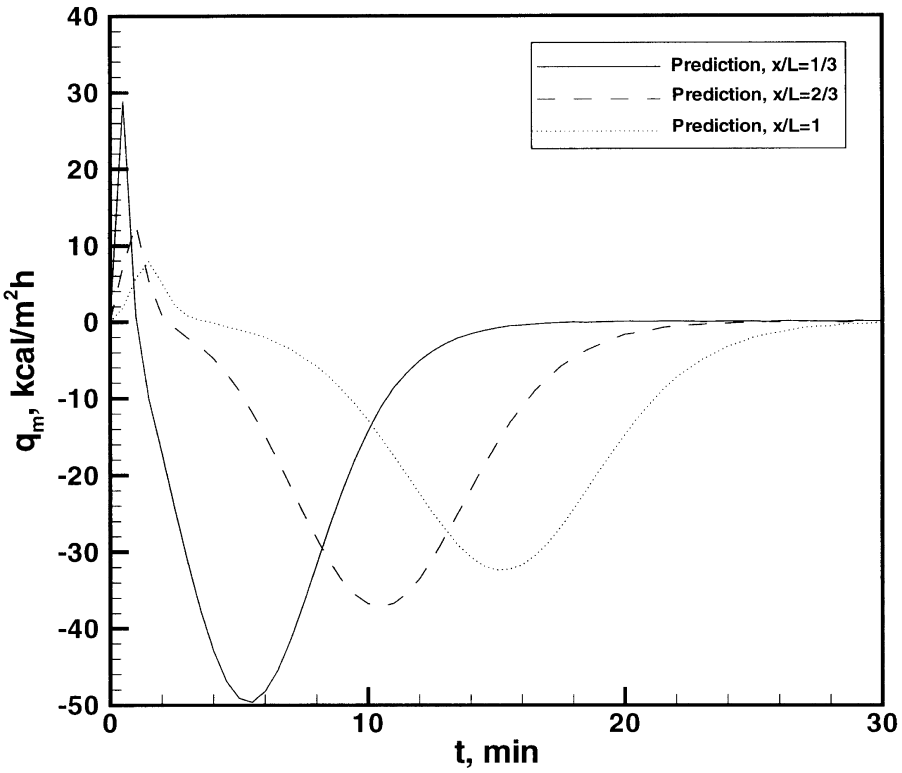

Fig. 5. Theoretically predicted latent heat fluxes (due to adsorption/desorption) for $Re_{D_h} = 75$.

of latent heat fluxes is approximately 35% larger than that of sensible ones. It is clear that the same general trends are exhibited by the numerical results at each instant of time. The latent heat fluxes are negative close to the inlet of the channel indicating desorption, and their maximum negative values are larger and are reached sooner (compare curves for $t = 0.5$ min and $t = 8.0$ min, for example). Further downstream (e.g., $x/L > 0.58$ for $t = 2$ min), readsorption of the earlier released adsorbate occurs and, therefore, the latent heat fluxes become positive. This kind of behavior of latent heat fluxes is completely consistent with distributions of the adsorption/desorption induced transverse mixture velocity at the wall presented in Fig. 6.

The sensible heat fluxes depicted in Fig. 9 remain positive everywhere along the tube. They are larger at the locations where desorption takes place, because heat is consumed at the gas/solid interface and the wall temperature decreases. This results in an increase of the temperature difference between the mixture bulk and channel walls and, consequently, leads to an enhancement of the sensible heat transfer. The opposite is true at the locations along the tube wall where adsorption occurs.

The local convective Nusselt number distributions have been calculated at several instants of time [14]. The results clearly show that the local Nusselt numbers are strongly non-uniform and behave differently at different times. As expected, the local Nusselt numbers decrease at locations where desorption occurs, because of the blowing effect associated with the negative (away from the wall) desorption induced velocities (Fig. 6). In contrast, the positive transverse velocities at the wall induced by adsorption enhance the local heat convective transfer. When desorption is strong and the negative transverse velocity at the wall is relatively large, the local Nusselt number can become even negative [14], and the concept becomes useless. From these observations one can conclude that reporting the local Nusselt numbers in the conjugate problems combined with surface physicochemical interactions such as adsorption/desorption appears to be meaningless. Instead, the local heat fluxes must be presented.

It is also important to emphasize that predicted instantaneous local Nusselt numbers differ significantly from the steady state values obtained from the empirical correlation [14]. It means that such correlations for the Nusselt number are not appropriate to define the local heat and mass transfer rates between the mixture and the

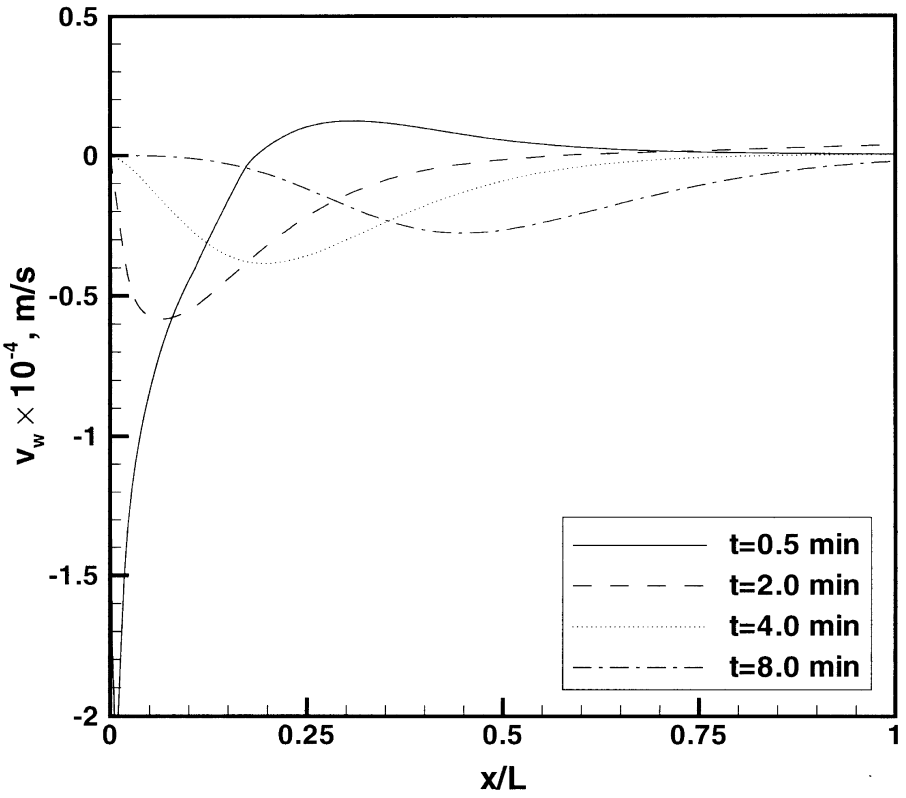

Fig. 6. Instantaneous spatial distributions of the adsorption/desorption induced velocity at the wall at several different times.

adsorbent solid in a framework of one-dimensional models and can be used only because of lack of a better choice.

3.3. Heat/mass transfer and adsorption/desorption interactions

The boundary condition, eqn (14), states that adsorption/desorption of adsorbable species on the channel wall leads to the presence of the non-zero net mass flux at the gas/solid interface. The induced transverse gas velocity at the wall v_w is positive (i.e., directed towards the wall) if adsorption occurs and an equilibrium amount adsorbed increases ($\dot{\Gamma} > 0$). Clearly, the opposite is true in the case of desorption ($\dot{\Gamma} < 0$ and $v_w < 0$). Figure 10 depicts variations of the adsorption/desorption induced velocity with time at three locations along the channel. As expected, the adsorption/desorption induced velocity is several orders of magnitude smaller than the longitudinal component of the mixture velocity. During first several minutes of the process (for example, 4 min at the exit of the channel) the transverse velocity at the wall is positive owing to adsorption of adsorbable species on the solid wall. After that v_w changes the sign and becomes negative, indicating that temperature induced desorption takes place. Eventually, the adsorption/desorption induced velocity vanishes owing to establishment of global thermal and solutal equilibrium in the channel (for example, $t > 27$ min at the exit of the channel).

Figures 11 and 12 demonstrate the effect of the adsorption/desorption induced mass transfer (non-zero transverse velocity at the wall v_w) on heat and mass transfer in the adsorption column. The effect is quite dramatic. Neglecting the adsorption/desorption induced net mass flux at the wall (i.e., setting $v_w = 0$) during an adsorption swing ($0 < t < 4$ min) leads to significant overpredictions (by as much as 20%) compared to the experimental measurements [17] in the transient bulk temperatures (Fig. 11) and, consequently, to overprediction of the sensible heat fluxes (Fig. 12). The opposite is true during a desorption part of the process ($t > 4$ min). Furthermore, the timewise variation of bulk temperatures and sensible heat fluxes is not predicted correctly if the heat/mass transfer and adsorption/desorption interactions are not accounted for in the formulation of the interface boundary conditions. Neglect of the adsorption/desorption induced velocity at the wall affects the transient concentrations of adsorbable species and latent heat fluxes in a similar fashion [14] and, therefore, are not presented.

The reasons for this can be determined from the following considerations: First, during an adsorption swing

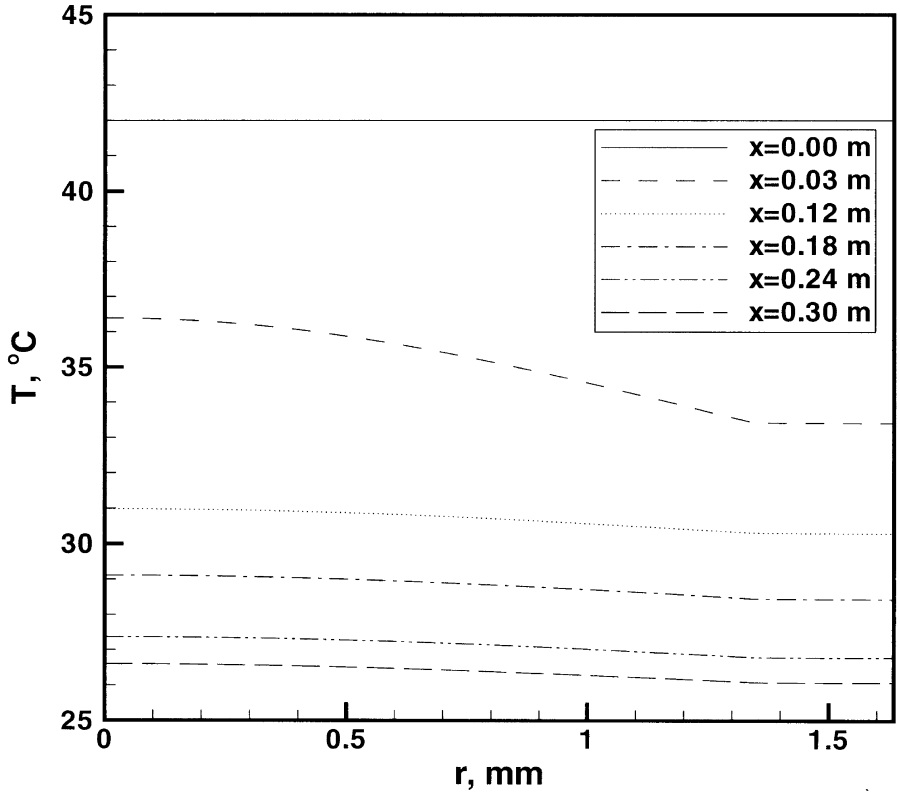

Fig. 7. Profiles of the predicted temperature at different locations along the channel for $t = 2$ min.

($0 < t < 4$ min) the warmer mixture from the stream core is advected towards the wall with a positive non-zero transverse velocity and, therefore, the gas/solid interface temperature increases. An increase in temperature leads to attenuation of the adsorption rate and, consequently, to a decrease in the amount of heat released due to adsorption [14]. Thus, an initial uptake of the bulk temperature is slower and its magnitude is smaller if the net adsorption induced mass flux at wall is accounted for compared to that if the adsorption induced velocity is neglected. Consequently, the weaker bulk temperature uptake in case $v_w \neq 0$ yields a smaller rate of change and the magnitude of the sensible heat flux (see Fig. 12). Second, during a desorption swing ($t > 4$ min), an adsorbable species released during a temperature induced desorption is swept away from the wall to the core of the stream by the negative desorption induced velocity (directed away from the wall). This prevents immediate readsorption of the adsorbable species and, therefore, leads to an increase in the rate of desorption [14]. In contrast to the expected trend, the sensible heat fluxes do not decrease but increase when blowing due to the negative (from the wall) desorption induced transverse mass flux occurs at the wall. This occurs because, despite a decrease in the local heat transfer coefficient due to blowing [14], the local temperature difference near the wall increases much more due to desorption induced decrease in the wall temperature. This results in an overall enhancement of sensible heat transfer rates when a desorption induced non-zero mass flux at the gas/solid interface is accounted for.

3.4. Effect of channel geometry on heat/mass transfer dynamics

In the baseline case (see preceding subsections), a square-shaped unit cell of a honeycomb adsorption column was replaced by a circular tube with an equivalent hydraulic diameter ($H = D_h = d$) (see Fig. 1). The question considered here is can a parallel plate channel be used as an adequate representation of the three-dimensional honeycomb unit cell?

One possibility would be to consider a parallel plate channel with spacing H equal to the internal width of the unit cell d. At the same time, using purely hydrodynamic arguments, one would be tempted to suggest that the parallel plate channel should have the width H such as the channel hydraulic diameter ($= 2H$) is equal to the hydraulic diameter of the unit cell $D_h = d$ or, in other words, $H = D_h/2$. To clarify these matters, numerical

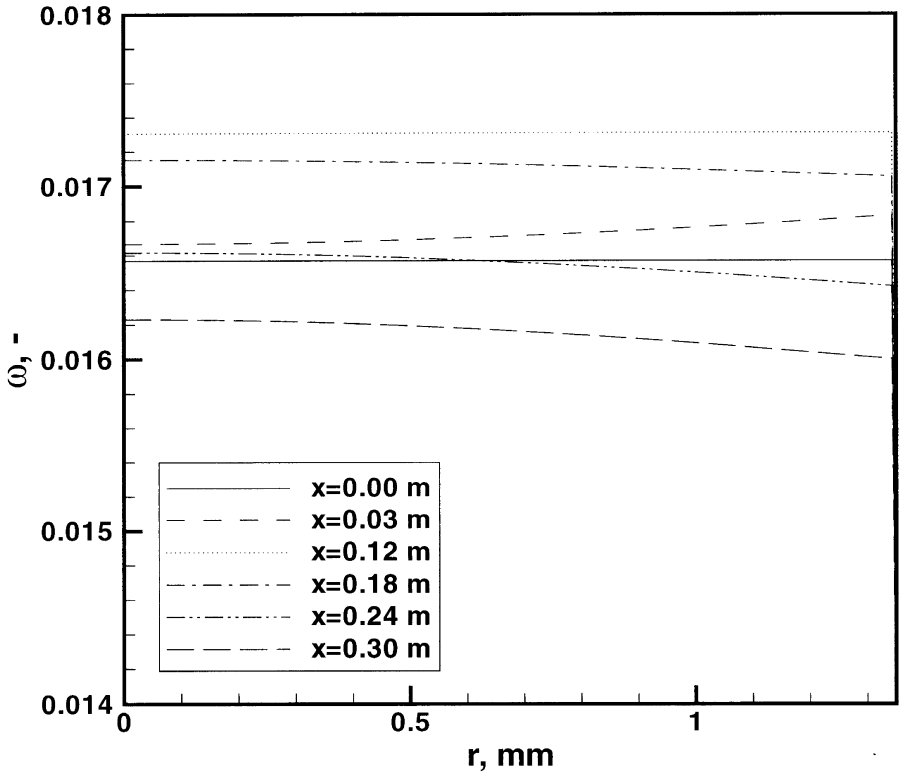

Fig. 8. Profiles of the predicted adsorbable species mass fraction at different locations along the channel for $t = 2$ min.

simulations of heat/mass transfer and adsorption/desorption dynamics have been performed for both cases. Figures 13 and 14 compare transient measurements of the bulk temperatures and local sensible heat fluxes with the theoretical predictions obtained for the circular tube ($H = D_h$), and for the parallel plate channels with two different widths of $H = D_h$ and $H = D_h/2$. The results clearly indicate that the theoretical predictions for the circular tube and the parallel plate channel with spacing $H = D_h$ lie very close to each other and also agree very well with the experimental data, whereas the numerical results obtained for the parallel plate channel with $H = D_h/2$ do not agree with the experimental data.

In order to explain the findings one should recall that adsorption is a surface phenomena. Therefore, it is critically important that the real three-dimensional system (honeycomb unit cell) and a two-dimensional channel which is employed to replicate the real system should have the same or, at least, approximately the same total specific surface area available for adsorption per unit volume of the solid adsorbent. Let us calculate the specific surface area for each of the four cases:

Square-shaped unit cell ($H = D_h = d$ and $w = t$):

$$A_{\square} = \frac{4H}{(H+w)^2 - H^2} = \frac{2}{t(1+t/2D_h)} \tag{19}$$

Circular tube ($H = D_h =$ d and $w = t$):

$$A_{\bigcirc} = \frac{\pi H}{(\pi/4)[(H+w)^2 - H^2]} = \frac{2}{t(1+t/2D_h)} \tag{20}$$

Parallel plate channel ($H = D_h = d$ and $w = t$):

$$A_{\parallel}(H = D_h) = \frac{1}{w/2} = \frac{2}{t} \tag{21}$$

Parallel plate channel ($H = D_h/2 = d/2$ and $w = t/2$):

$$A_{\parallel}(H = D_h/2) = \frac{1}{w/2} = \frac{4}{t} \tag{22}$$

Here d and t stand for the internal width and the thickness of the wall of the honeycomb unit cell, respectively [13, 14]. Equations (19) and (20) indicate that the specific surface area of the unit cell $A_{\square}$ is equal to that of the circular tube $A_{\bigcirc}$; therefore, an excellent agreement is expected between experimental data and numerical predictions obtained for the circular tube.

The expression for the specific surface area in the case of a parallel plate channel with width $H = D_h$, equation

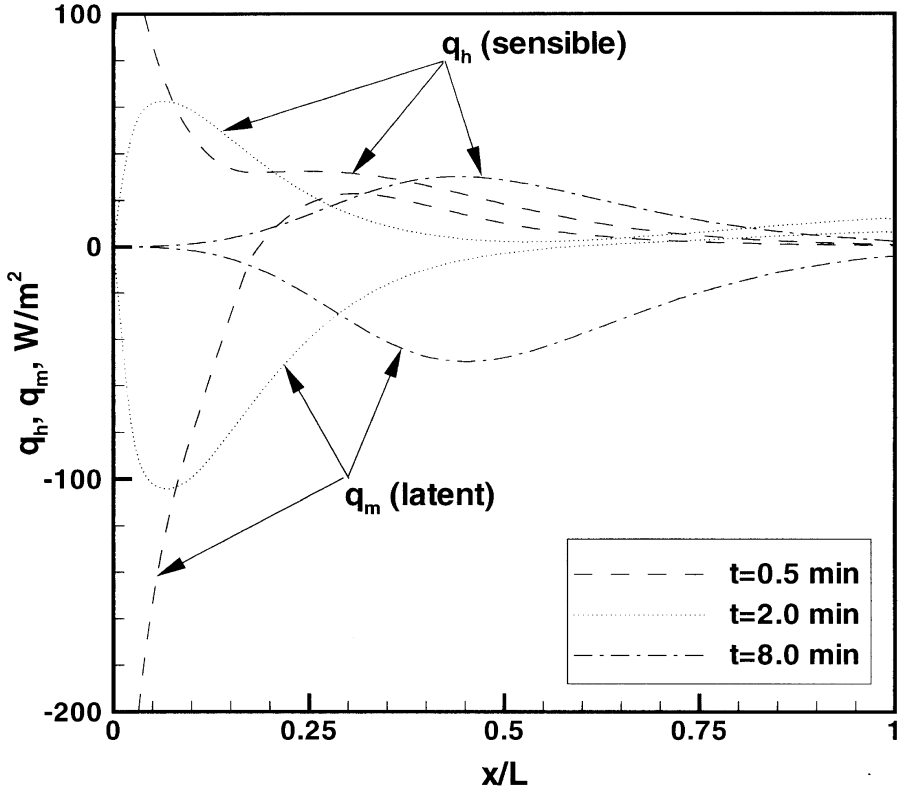

Fig. 9. Instantaneous spatial distributions of the sensible and latent heat fluxes at the wall at several different times.

(21), yields a larger value than the surface area calculated from the two preceding expressions, equations (19) and (20), due to the presence of the correction term $(1+t/2D_h)$ in the denominator. For the particular honeycomb geometry considered, the thickness of the wall ($t = 0.58$ mm) is almost an order of magnitude smaller than the hydraulic diameter ($D_h = d = 2.69$ mm), and this produces the value of the correction term very close to the unity ($= 1.1078$). Since $A_{\parallel}(H = D_h)$ is only slightly greater than $A_{\bigcirc}$ (i.e., by factor of 1.1078), the numerical predictions for these two cases are barely different. As expected, the slightly larger value of the specific surface area for the parallel plate channel results in stronger adsorption/desorption and, consequently, slightly greater adsorption induced temperature uptake (Fig. 13) and greater sensible heat fluxes (Fig. 14).

The specific surface area for the parallel plate channel with a smaller spacing ($H = D_h/2$) is at least twice as large as the surface area obtained in each of the three previous cases [compare eqn (22) with equations (19)–(21)]. It means that the rates of adsorption/desorption are artificially increased more than two-fold. This leads to the significant overprediction of the transient bulk temperatures and sensible heat fluxes.

The analysis presented in this subsection reveals the critical importance of correct accounting for the total specific surface area available for adsorption/desorption when a two-dimensional model is employed to simulate heat/mass transfer and adsorption dynamics in the three-dimensional system.

4. Conclusions

A transient two-dimensional analysis of heat/mass transfer and adsorption/desorption has been developed in order to gain an improved understanding of the honeycomb adsorption column dynamics. The simplified statistical mechanics (SLD) model has been used to simulate an adsorption/desorption on the flat walls of the honeycomb column.

The local nonlinear interactions between heat/mass transfer and adsorption/desorption as the surface phenomena have been investigated using a transient two-dimensional theoretical model developed. The appropriate surface boundary conditions for heat and mass transfer in the presence of adsorption/desorption have been formulated. Based on the results obtained, the following conclusions can be drawn:

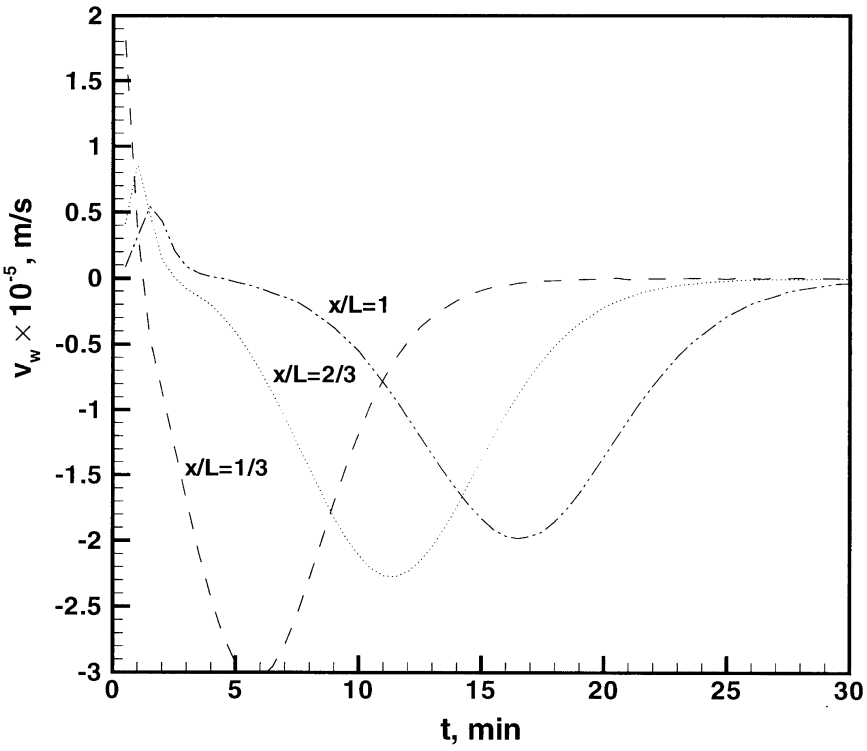

Fig. 10. Transient variations of the theoretically predicted adsorption/desorption induced velocity at different locations along the channel.

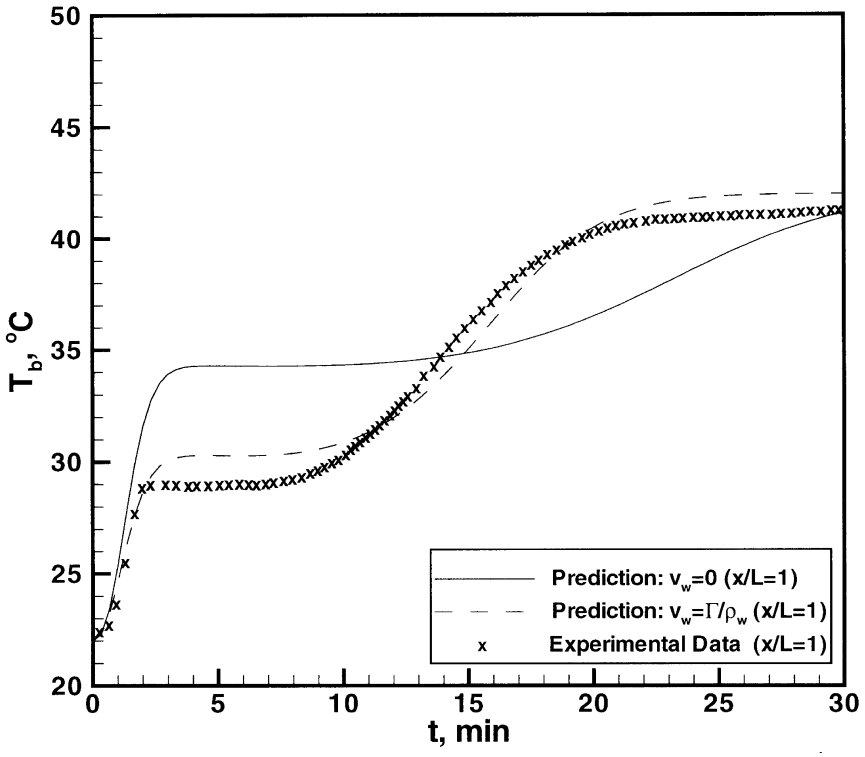

Fig. 11. Effect of the adsorption/desorption induced mass transfer on the theoretically predicted transient bulk temperature distributions.

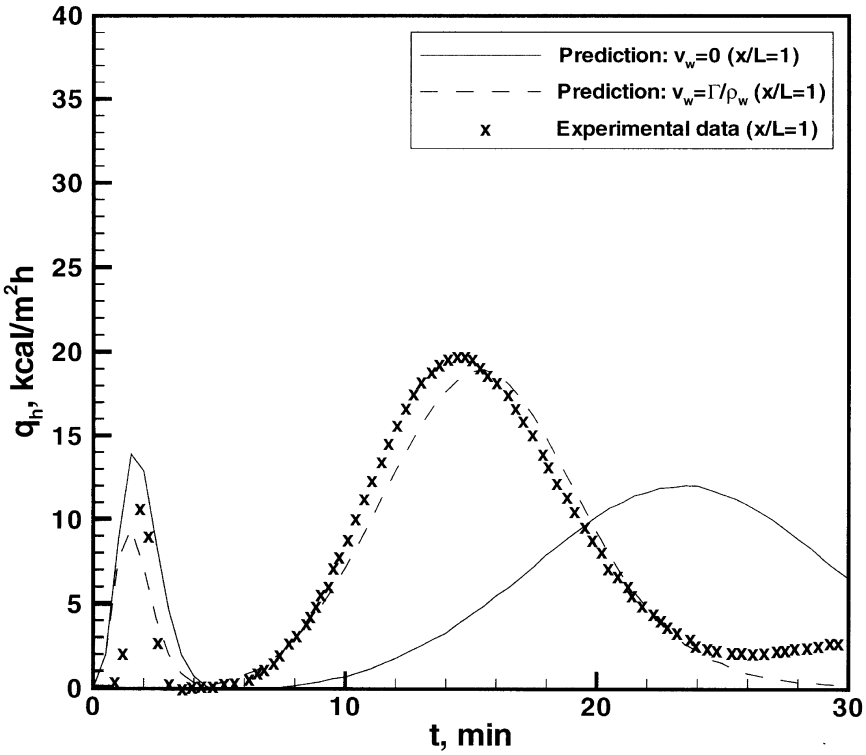

Fig. 12. Effect of the adsorption/desorption induced mass transfer on the theoretically predicted transient sensible heat fluxes.

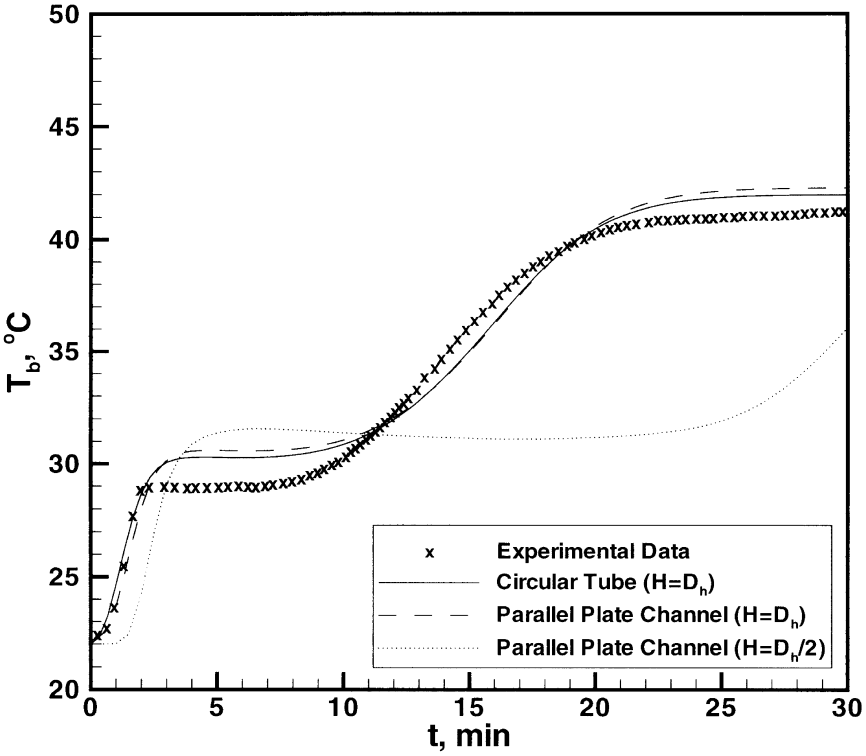

Fig. 13. Effect of the channel geometry on the theoretically predicted transient bulk temperature distributions at the exit of the channel ($x/L = 1$).

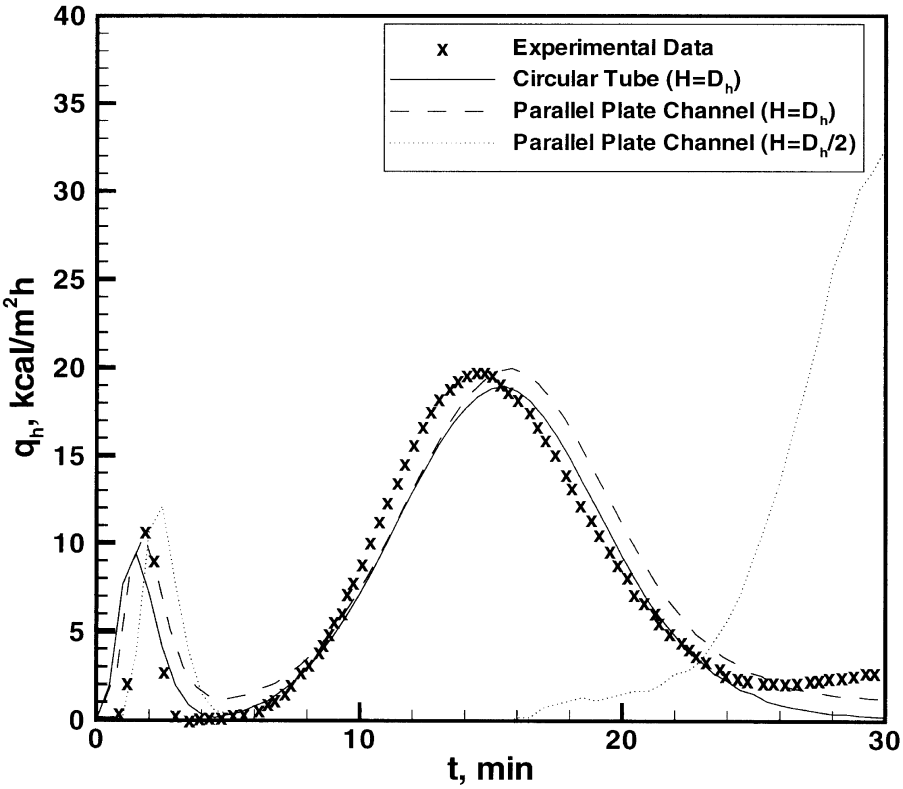

Fig. 14. Effect of the channel geometry on the theoretically predicted transient sensible heat fluxes at the exit of the channel ($x/L = 1$).

- The two-dimensional heat and mass transfer model combined with the SLD adsorption isotherm is fully capable of adequately predicting heat/mass transfer rates and adsorption/desorption dynamics in the honeycomb adsorbent.
- Comparison of results of numerical simulations of the system dynamics with available experimental data clearly indicates the vital importance of accounting for the non-zero net mass flux at the channel walls due to the presence of adsorption/desorption.
- The calculated instantaneous local sensible and latent heat fluxes are strongly nonuniform. In the case of adsorption, a decrease in the bulk-to-wall temperature difference is larger than an increase in the local heat transfer coefficient. This results in a decrease in the magnitude of the sensible heat fluxes. The opposite is true in the case of desorption.
- The local convective heat transfer coefficients become negative at the locations where desorption occurs. Thus, reporting the coefficients in the conjugate heat and mass transfer problems combined with the surface physicochemical reactions such as adsorption/desorption was found to be meaningless. Instead, the results must be presented in terms of the local heat fluxes.
- The correct accounting for the total specific surface area available for adsorption/desorption is critically important when a two-dimensional model is employed to simulate heat/mass transfer and adsorption dynamics in the three-dimensional system.

Acknowledgements

The authors wish to thank Dr A. Yamada, Mitsubishi Heavy Industries, Ltd, Nagasaki Research and Development Center, for providing unpublished data on the dynamic behavior of the honeycomb adsorbent and for numerous technical discussions. Partial financial support for this work was provided by Mitsubishi Heavy Industries, Ltd and is gratefully acknowledged.

References

[1] D. Ruthven, Principles of Adsorption and Adsorption Processes, Wiley & Sons, New York, 1984.
[2] M. Suzuki, Adsorption Engineering, Elsevier, Amsterdam, 1990.

[3] S. Gregg, K. Sing, Adsorption, Surface Area and Porosity, Academic Press, New York, 1982.
[4] S. Ülkü. Heat and mass transfer in adsorbent beds, in: S. Kakac et al. (Eds.), Convective Heat and Mass Transfer in Porous Media, Kluwer Academic Publishers, Dordrecht and Boston, 1991, pp. 695–724.
[5] A. Fedorov, R. Viskanta, Heat and mass transfer aspects of gas separation by adsorption. Journal of the Heat Transfer Society of Japan, 36 (1997) 4–11.
[6] S. Farooq, D. Ruthven, Heat effects in adsorption column dynamics. 1. comparison of one- and two-dimensional models, Industrial Engineering Chemistry and Research 29 (1990) 1076–1084.
[7] K. Gukov, E. Ukina, V. Mironov, Numerical analysis of the multicomponent adsorption in the fixed porous bed, in: A.I. Leontiev et al. (Eds.), Proceedings of the 1st Russian National Heat Transfer Conference, vol. 7, MPEI Publisher, Moscow, Russia, 1994, pp. 77–82.
[8] A. Mohamad, A. Yamada, R. Viskanta, Mathematical modeling of adsorption and desorption in a fixed bed, in: L. Fletcher, T. Aiahara (Eds.), Proceedings of the ASME/JSME Thermal Engineering Joint Conference, vol. 3, ASME, New York, 1995, pp. 305–312.
[9] H. Bart, R. Germerdonk, P. Ning, Two-dimensional non-isothermal model for toluene adsorption in a fixed-bed adsorber, Chemical Engineering and Processing 36 (1996) 57–64.
[10] G. Dubrovskiy, Microscopic models of heat and mass transfer for growing adsorption films. Heat Transfer Research 24 (1992) 785–795.
[11] E. Eckert, R. Drake, Analysis of Heat and Mass Transfer, McGraw-Hill, New York, 1972.
[12] B. Rangarajan, C. Lira, R. Subramanian, Simplified local density model for adsorption over large pressure ranges, AIChE Journal 41 (1995) 838–844.
[13] A. Fedorov, R. Viskanta, Heat/mass transfer and adsorption dynamics in a honeycomb adsorbent: application of the simplified local density model, in: S. Fukusako, K. Hijikata (Eds.), Proceedings of the 45th Oji International Seminar, Tomakomai City, Hokkaido, Japan, 1997, pp. 1–9.
[14] A. Fedorov, Combined heat and mass transfer and adsorption dynamics in a honeycomb adsorbent, Ph.D. thesis, Purdue University, West Lafayette, IN, 1997.
[15] S.V. Patankar, Numerical Heat Transfer and Fluid Flow, Hemisphere, Washington, DC, 1980.
[16] A. Mohamad, R. Viskanta, Application of low Reynolds number k–ε turbulence model to buoyant and mixed flows in a shallow cavity, in: T.S. Chen, T.Y. Chu (Eds.), Fundamentals of Mixed Convection, vol. HTD-213, ASME, New York, 1992, pp. 43–54.
[17] A. Yamada, Dynamic behavior of a honeycomb adsorbent, Personal communication, Mitsubishi Heavy Industries, Ltd, Hagasaki Research and Development Center, Japan, 1994.